

New applications of Bayesian optimization based on element mapping to design high-capacity NASICON-type cathode of sodium-ion battery

Sanghyeon Park^{1, 2}, Yoonsu Shim¹, Junpyo Hur¹, Dongmin Jeon², Jong Min Yuk^{1*}, Chan-Woo Lee^{2*}

1 Department of Materials Science and Engineering, Korea Advanced Institute of Science and Technology, Daejeon 34141, Republic of Korea

2 Energy AI & Computational Science Laboratory, Korea Institute of Energy Research, Daejeon 34129, Republic of Korea

Keywords: Data-driven materials design, Bayesian optimization, Sodium ion battery, Density functional theory

Abstract

Sodium-ion batteries are emerging as promising alternatives to lithium-ion batteries due to the abundance of sodium resources. $\text{Na}_3\text{V}_2(\text{PO}_4)_2\text{F}_3$ (NVPF), a cathode material for sodium ion batteries, is attracting attention from its rate capability and high working voltage, but its low discharge capacity is one of the challenges. In this work, we aim to design a high-capacity NASICON-type cathode of sodium-ion battery by discovering element combinations that can stabilize the sodium excess phase in NVPFs. For the efficient discovery of element combinations, we propose a Bayesian optimization-based algorithm for chemical composition discovery. Specifically, we propose an element mapping technique to solve the limitation of Bayesian optimization in discovering chemical composition. By constructing a chemical space

applicable to Bayesian optimization through element mapping and optimizing the constructed chemical space, we found optimal binary element combinations. This work not only offers insights into designing high-capacity cathodes, but also demonstrates the efficacy of the proposed algorithm in data-driven materials design.

1. Introduction

In response to the growing demand for energy storage devices such as electric vehicles and energy storage systems (ESS), lithium-ion batteries have seen widespread adoption. However, with growing concerns about limited lithium resources and costs, sodium-ion battery (SIB) is emerging as a possible alternative based on abundant sodium resources[1-3]. Unfortunately, due to the chemical differences between lithium and sodium ion, electrode materials designed for lithium-ion batteries are not suitable for sodium ions, so it is necessary to re-design suitable electrode materials for SIB. Among the sodium superionic conductor (NASICON) structures[4-6], $\text{Na}_3\text{V}_2(\text{PO}_4)_2\text{F}_3$ (NVPF) is one of the emerging cathode material of SIBs[7, 8], which has the advantages of high-rate capability for fast charge/discharge and high working voltage. However, its low energy density needs to be addressed. This is because even if there is space to accommodate additional sodium in the lattice, which enable form a sodium excess phase ($x = 4$ in $\text{Na}_x\text{V}_2(\text{PO}_4)_2\text{F}_3$) by storing additional sodium in the lattice, the thermodynamic instability of the sodium excess phase leads to a working voltage of sodium excess phase outside the voltage window. From this reason, the sodium excess phase does not participate in cell operation making energy density loss. This phenomenon suggests that high-capacity NVPF can be designed by stabilizing the sodium excess phase.

One of the strategies to stabilize sodium excess phase thermodynamically is replacing vanadium in NVPF structure by the binary element combinations composed of transition

metals ($\text{Na}_x\text{M}(\text{PO}_4)_2\text{F}_3$, $\text{M}=\text{M1}_{2.00-y}\text{M2}_y$, NMPF). Unfortunately, exploring the chemical space created by considering all possible chemical components and compositions using conventional techniques such as grid search is time-consuming and expensive due to the large number of cases and complexity of chemical space.

Recently, Bayesian optimization [9-11] based on the Gaussian process [12, 13], a probabilistic approach to find the optima in unknown functions, has attracted a lot of attention to discover optimal materials in the chemical space. Bayesian optimization is effective to find optima with minimal observations for functions requiring high costs for observations. For this reason, Bayesian optimization is actively applied in material design to reduce the cost of experiments and simulations including density functional theory (DFT) calculations [14-18]. However, there are limitations that the Gaussian process, which is surrogate model in Bayesian optimization, is designed for continuous inputs meaning that it is difficult to cover discontinuous inputs such as element (chemical components). There is also no proper rule to define the chemical space containing chemical component and composition.

In this study, we propose an element mapping that can convert the discontinuous property of element into a continuous input by assigning continuous value to element and simultaneously create a non-complex chemical space. We also analyzed which input is suitable for creating easily predictable chemical space with the element mapping and discovered optimal element combinations re-positioning all working voltages of NVPF within the voltage window (2.5-4.3V) with the algorithm for new application of Bayesian optimization based on element mapping. In addition, compared to previous deep learning-based discovery methods, we found more optimal element combinations without any initial training dataset[19]. Furthermore, the analysis with DFT calculations revealed the stabilization mechanism of the sodium excess phase.

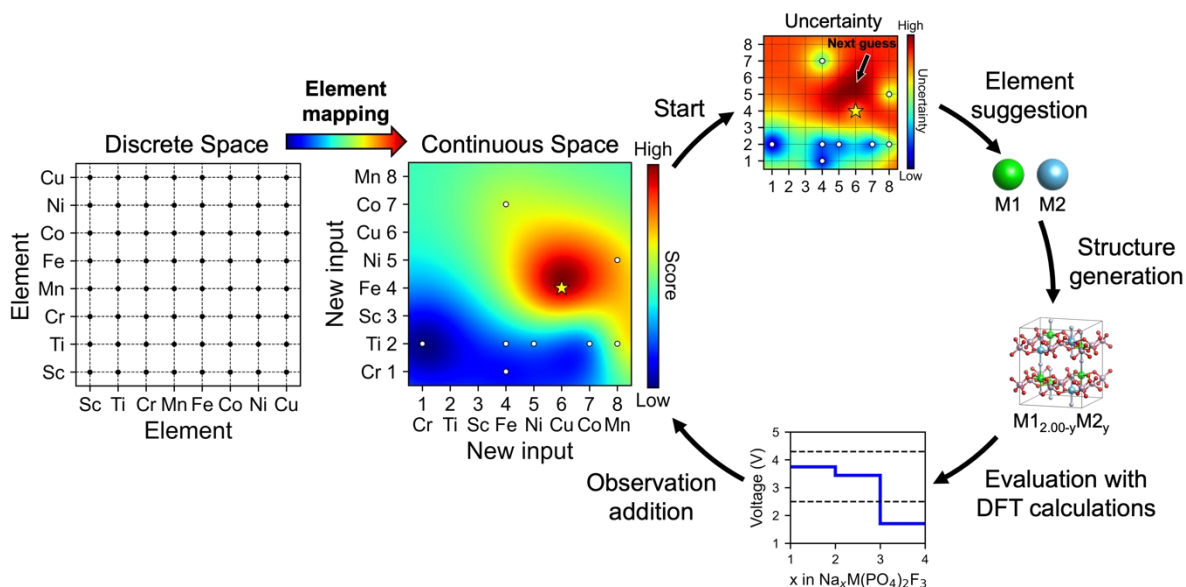


Fig. 1 | Scheme of Bayesian optimization-based optimal elements discovery algorithm

2. Results & discussion

2.1 Algorithm Framework

Fig. 1 illustrates the overall schematic of the Bayesian optimization-based algorithm for discovering optimal binary element combinations that stabilize the sodium-excess phase of NVPF, thereby repositioning all working voltages within the voltage window of 2.5-4.3V. Generally, Bayesian Optimization is used to find the optimal solution of an objective function by predicting with a surrogate model and suggesting the next guess with an acquisition function. However, Gaussian Processes, commonly adopted in surrogate models, are designed for smooth and continuous functions, making it challenging to identify optimal chemical components in discrete chemical spaces directly defined by elements. Furthermore, the method for constructing the chemical space is often unclear.

To address this issue, we introduce an element mapping technique. Element mapping is

assigning each element to its continuous value, which transforms the discrete space directly created by the elements into a continuous one. The acquisition function in Bayesian optimization suggests specific values in chemical space as its next guess, and these values are then converted into element combination with element mapping. Based on the proposed element combination, structures are created considering all possible compositions rather than optimizing, since the number of possible cases is small. For example, from the 8 sites for M1 and M2 in the $\text{Na}_3\text{M}_{1.00-y}\text{M}_{2y}(\text{PO}_4)_2\text{F}_3$ (Fig. 2a), the possible chemical compositions replacing vanadium in NVPF are $\text{M}_{1.75}\text{M}_{2.25}$, $\text{M}_{1.50}\text{M}_{2.50}$, $\text{M}_{1.25}\text{M}_{2.75}$, $\text{M}_{1.00}\text{M}_{3.00}$, $\text{M}_{0.75}\text{M}_{3.25}$, $\text{M}_{0.50}\text{M}_{3.50}$ and $\text{M}_{0.25}\text{M}_{3.75}$. To consider the arrangement between the proposed elements in same composition, the relative energies of the possible arrangements in the same composition were compared by DFT calculations, and the most stable structure was selected as a representative structure for the proposed chemical composition. From this representative structure, the sodiation process is simulated through DFT calculations to obtain voltage profiles based on the Nernst equation[20]. These voltage profiles are then converted into single values using a scoring function (Fig. 2b and 2c). From this, the highest score from various compositions and components represents the suggested element combination. This observation, based on DFT calculations, is added to the algorithm. The algorithm iterates this process to find the optimal element combinations with the least number of observations.

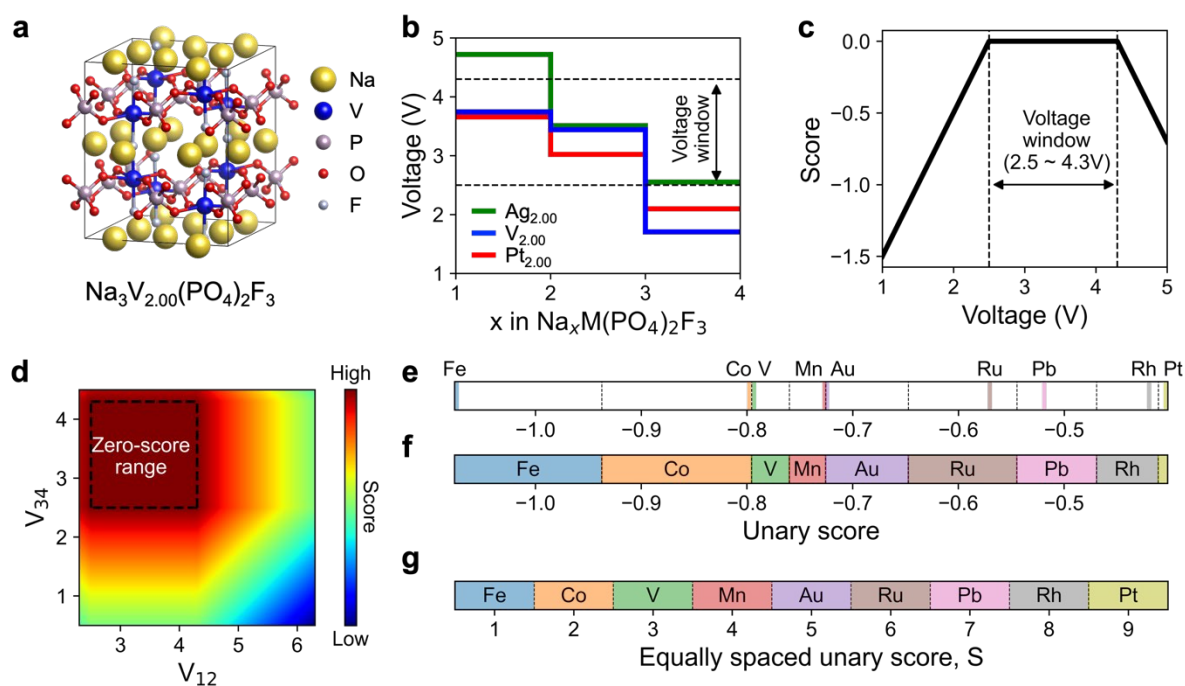


Fig. 2 | Preprocess for evaluating method and the element mapping. **a** Crystal structure of NVPF. **b** DFT calculations-based theoretical voltage profiles of pure NVPF and Ag and Pt substituted NVPF. Scoring function in **c** one-dimension and **d** two-dimension. **e** Unary scores of substituted NVPF with example elements. **f** The regions defined with the median of the unary scores. **g** equally spaced unary score.

2.2 Creating chemical space element mapping

Fig. 2 shows details of the scoring function and element mapping. NVPF structures with different sodium concentrations are labeled as Na₁, Na₂, Na₃, and Na₄, corresponding to the amount of sodium in the 1×1×1 unit cell (Fig. 2a and Supplementary Fig. 1). DFT calculations were performed on these structures, and theoretical voltage profiles were derived with the Nernst equation (Fig. 2b). The working voltages in the theoretical voltage profiles for the (Na₁, Na₂), (Na₂, Na₃), and (Na₃, Na₄) structures are specified as V_{12} , V_{23} , and V_{34} . To create a criterion for the Bayesian optimization to evaluate voltage profiles from suggested element

combination, we define a scoring function (Fig. 2c). The function returns a score of zero when working voltage is within the voltage window and gives a penalty when the working voltage deviates from the voltage window. The total score of the voltage profile is defined as the sum of the scoring function values of V_{12} , V_{23} , and V_{34} . Fig. 2d shows a two-dimensional score space composed of only V_{12} and V_{34} and represents the zero-score range, which is the region with the highest score. In the practical optimization process, a three-dimensional score space is formed consisting of V_{12} , V_{23} and V_{34} . This scoring method aims to identify the optimal element combination that bring all working voltages of the structure within the zero-score range. To successfully find the optimal element combinations with the minimum number of observations, the chemical space defined by the input and the scoring function (output) should be easy to predict. This means that there should be fewer regions with steep gradients within the chemical space [ref]. If we consider the chemical space as a function, then input and the scoring function should be highly correlated to avoid abrupt gradient regions. Because the scoring function evaluate the position of working voltage, the scoring function are highly connected to sodiation process. From this reason, the input should be correlated with the sodiation process.

Here, we introduce unary score as an appropriate input. The unary score is a value representing the score of a structure where all vanadium in NVPF is replaced by the element. From this, it is possible to capture the properties of sodiation process as a value when the element is within the framework of an NVPF. For example, the theoretical voltage profiles of pristine NVPF and the fully substituted NVPF with Pt and Ag are shown in Fig. 2b, and the order of their unary score is Pt, V and Ag (-0.40, -0.79 and -2.01, respectively). In Fig. 2e, the unary scores of nine example elements are described in one-dimensional continuous space. Within the continuous space, the regions are defined with the median of the unary scores as the boundary (Fig. 2f). By equally spacing these regions (Fig. 2g), the equally spaced regions are assigned to the elements and the elements can be mapped to the specific value. The technique designs the

smooth chemical space with a low gradient by presenting the appropriate array of elements (inputs) that are highly correlated with the scoring function and evenly spacing the regions mapped to the elements.

Even if not the unary score, any value that can represent an element can be used for element mapping. One example is electronegativity, which represents the tendency to attract electrons and is already used as an input in machine learning models[21-23]. Because the role of transition metals in NMPF is to store electrons during sodiation process, electronegativity can be useful for element mapping. However, the unary score has a higher correlation with the scoring function than electronegativity. Because the unary score can directly capture not only the role of the transition metal in the NVPF environment which are not covered by electronegativity alone, but also the relaxation effects and changes in the electronic structure. To investigate how the correlation between the sodiation process and input facilitates the prediction of chemical space, 35 elements were mapped using the equally spaced unary score (S), equally spaced electronegativity (X), and equally spaced atomic number (Z) to create inputs.

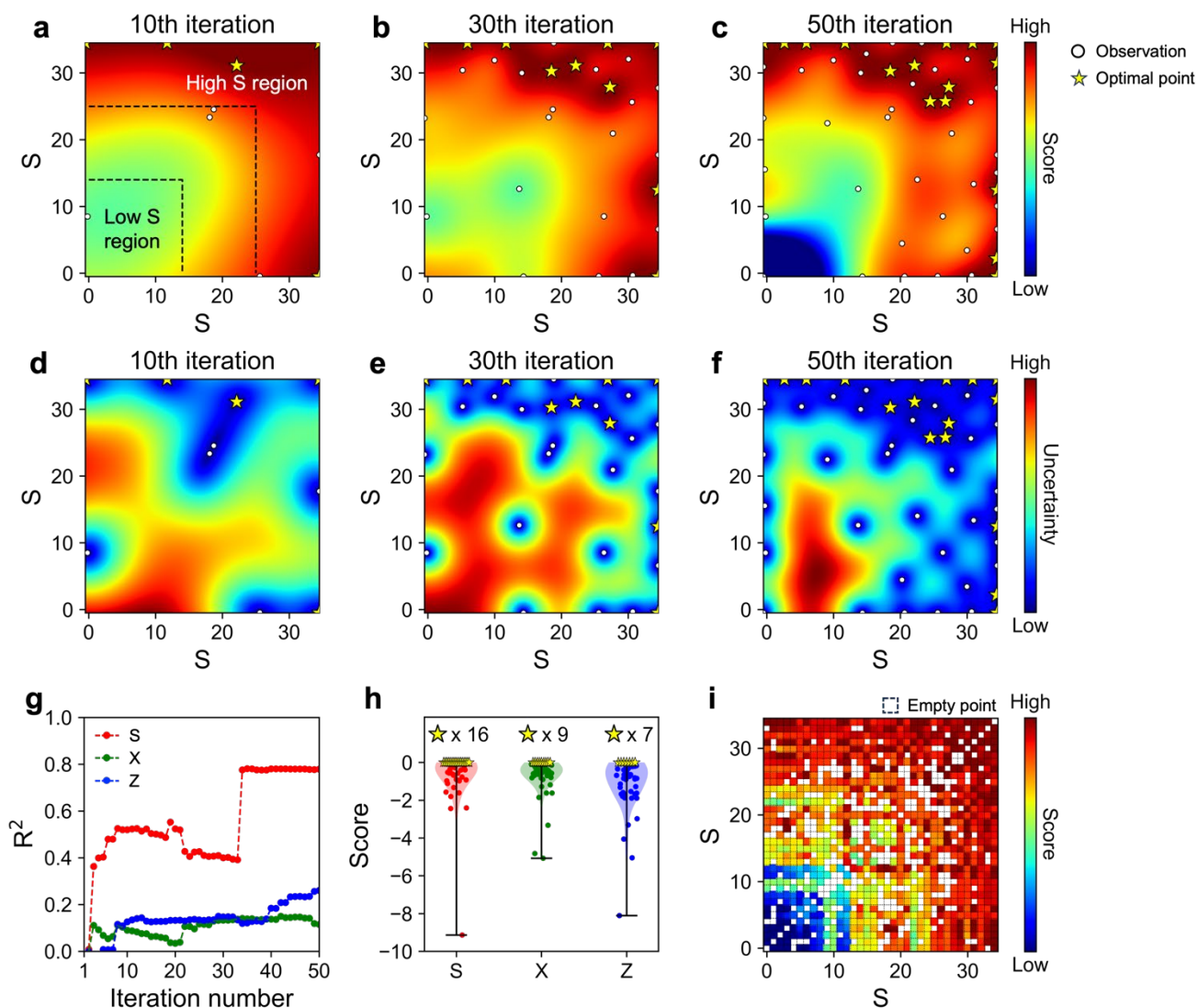


Fig. 3 | The process and results of exploring binary element combination. Predicted chemical space at **a** 10th, **b** 30th and **c** 50th iterations. Uncertainty at **d** 10th, **e** 30th, **f** 50th iterations. White circle and yellow star indicate observation and optimal point. The predicted score and uncertainty are represented by colors. **g** R^2 values of predicted chemical space evaluated by each ground truth with different mapping features at each iteration. **h** Violine plot of observations with different inputs. **i** Ground truth defined by the collected observation data. White area indicates empty point.

2.3 Bayesian optimization for optimal binary element combination

Fig. 3 shows the process and results of exploring the optimal binary element combinations in a two-dimensional continuous chemical space, transformed with element mapping by equally spaced unary score (S). The chemical space is formed with 35 elements and the total number of cases is 630 (${}_{35}C_1 + {}_{35}C_2$). The predicted chemical spaces by surrogate model at 10th, 30th, and 50th iterations are shown in Figs. 3a-c. In the predicted chemical space at 10th iteration steps, there is a preliminary tendency for low S region to have low scores and high S regions to have high score. As the iteration progresses, the tendency is becoming clear. As the iterations progress, the trend becomes clearer, and it has been found that there are more observations in the high S region with high scores rather than low S region. It means that the exploitation to observe near the high score observations progressed properly. Figs. 3d-f show the uncertainty from 95% confidence interval at 10th, 30th, and 50th iterations and the maximum and minimum values of uncertainty are determined in each iteration step. As the iterations progress, uncertainty within the chemical space has been reduced overall. Specifically, at 50th iterations, the regions where uncertainty is still high are the regions with low scores in the predicted chemical space and there are relatively few observations. This means that the algorithm has mainly explored regions with high scores. However, given that there are observations in the 50th iteration in areas where the algorithm already judged the score to be low at 30th iteration, it is inferred that there has been progress in exploration as well as exploitation.

Fig. 3i shows the ground truth of chemical space formed with S from the observation data for an overview of the chemical space and quantification of the predictions made by the Gaussian process. The comparison of the ground truth and predicted chemical space at 50th iterations shows that the chemical space predicted by the Gaussian process is qualitatively similar to the ground truth. For quantitative analysis, the R-square value (R^2) between predicted chemical

space and ground truth was also determined (Fig. 3g). The R^2 increases until the 10th iteration and then gradually decreases to the 30th iteration. This is due to the lack of observations in the low S region when comparing the predicted chemical space at the 30th iteration with the ground truth. Then, after the observations in the low S region with exploration process, a high R^2 (0.774) is achieved at the 50th iteration.

Fig. 3h shows that total 16 optimal points and 14 element combinations are discovered without overlapped element combinations (Os-Pb, Pd, Hf-Pd, Mo-Pd, Pd-V, Mn-V, Pd-Re, Mo-Pd, Ag-Ru, Pd-W, Co-Ir, Pb-Pd, Co-V and Pd-Ta). Total 24 compositions are included in element combinations. Each element combinations were then reduced to the 16 element combinations by DFT calculations again with tight convergence criteria (Supplementary Fig. 5).

Supplementary Fig. 6 shows the process and results of Bayesian optimization with X and Z. As we mentioned before, X is slightly correlated with the scoring function in terms of quantifying the degree to which the transition metal receives electrons, and Z is less correlated. Supplementary Fig. 6a and 6b show predicted chemical space formed with X and Z at 50th iteration. In each chemical space, more observations were made in the higher scoring areas, indicating that the optimization was successful even if it was only in a narrow area. However, the chemical space formed with X has an overall low uncertainty, whereas that formed with Z does not (Supplementary Fig. 6c and 6d). This is due to the smoothness of the chemical space caused by the difference in correlation with the scoring function. More specifically, the chemical space formed by X, which is relatively more correlated than Z, has an upward tendency (Supplementary Fig. 6e), meaning that the formed chemical space is smooth rather than complex. The tendency is close to the chemical space formed by S, which is highly correlated with the scoring function. However, there are also high gradient areas where the score changes rapidly, making it difficult for the surrogate model to predict. Similarly, the

chemical space formed by Z with low correlation is more complex, so the surrogate model is difficult to predict and there are areas that it misses. For these reasons, R^2 of predicted chemical space formed with X and Z is not only significantly low (0.118 and 0.258 at 50th iteration, respectively) than the case of S, but also the numbers of discovered optimal points are smaller (9 and 7 at 50th iteration, respectively) because there are many missed regions (Figs. 3g and 3h).

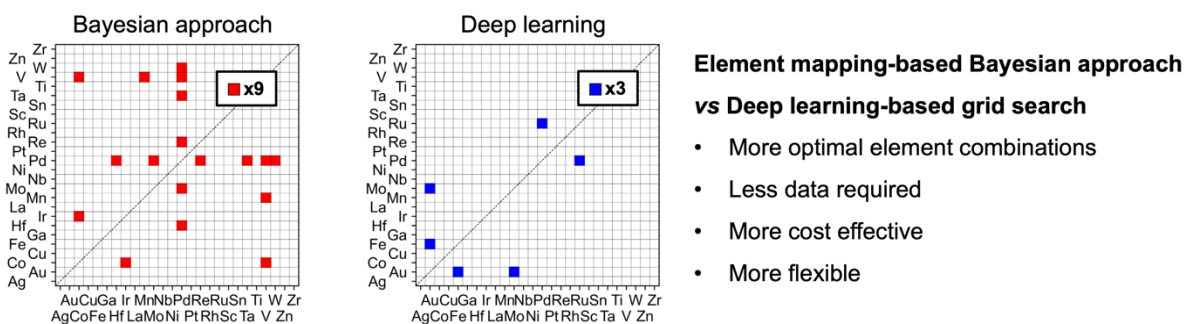


Fig. 4 | Schematic comparison of Bayesian approach and deep learning-based approach

2.4 Effectiveness of the Proposed Algorithm

Previously, materials screening studies have used deep learning models to directly predict material properties[24-27]. To confirm how the new application of Bayesian optimization is effective to find optimal element combinations, we compared our results with that of deep learning-based screening studies[19]. The deep learning model predicts the formation energy of $\text{Na}_x\text{M}_{12.00-y}\text{M}_2\text{y}(\text{PO}_4)_2\text{F}_3$ (NMPF) in a chemical space formed with 30 elements (Supplementary Fig. 9) where the total number of cases is 465 ($30\text{C}_1 + 30\text{C}_2$). Based on the predicted formation energy, the predicted working voltages of NMPF are adopted to the scoring function defined in this study (Figs. 2b and 2c) and a total of 27 predicted optimal points are

found. However, after validation process with DFT calculations with the tight convergence criteria, there are only four element combinations ($\text{Au}_{1.25}\text{Mo}_{0.75}$, $\text{Au}_{1.50}\text{Fe}_{0.50}$, $\text{Pd}_{1.25}\text{Ru}_{0.75}$ and $\text{Pd}_{1.50}\text{Ru}_{0.50}$). Based on overlapping candidate elements (Supplementary Fig. 7), the number of optimal element combinations found by the Bayesian approach is 9 and the number found by deep learning is 3. If we consider the composition, the 11 and 4 compositions are included in each element combinations, respectively (Fig. 4). In addition to the number of element combinations found, the proposed algorithm does not require initial training data essentially and has a low computational cost.

In terms of making a discrete property continuous, autoencoder and variational autoencoder (VAE) have been used to represent elements and molecules as latent space, which is a continuous vector space, and applied to Gaussian process[28, 29]. However, Gaussian process is not suitable for dealing with high-dimensional data, as it may lead to higher computational complexity and lower predictive power when learning and predicting high-dimensional latent space. So, it may be disadvantageous to use the Gaussian process to learn and predict high dimensional latent spaces, On the other hand, the dimension of the chemical space constructed by element mapping depends on the desired number of element types. Specifically, since this study attempted to discover optimal binary element combinations, a two-dimensional chemical space was formed. In addition, the latent space formed by autoencoder, and VAE is a space that machine learning model can read but humans have difficulty understanding. In contrast, because the chemical space formed by elemental mapping is based on material science knowledge, it can be used as input for machine learning models as well as intuitively understood by humans.

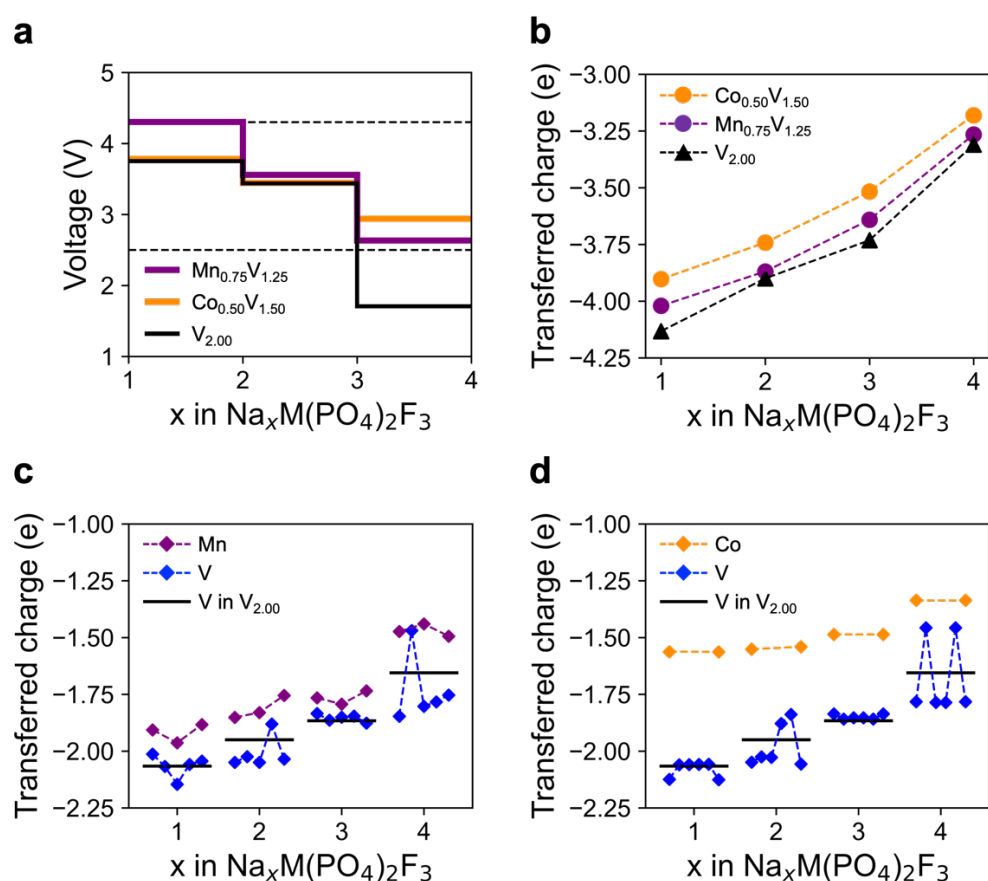


Fig. 5 | Analysis with DFT Calculations. **a** Theoretical voltage profiles of NMPF with $\text{Mn}_{0.75}\text{V}_{1.25}$ and $\text{Co}_{0.50}\text{V}_{1.50}$ and NVPF. **b** Bader charge analysis for transferred charge to $\text{Mn}_{0.75}\text{V}_{1.25}$ and $\text{Co}_{0.50}\text{V}_{1.50}$ in NMPF and $\text{V}_{2.00}$ in NVPF. Atomic Bader charge analysis for transferred charge to **c** $\text{Mn}_{0.75}\text{V}_{1.25}$ and **d** $\text{Co}_{0.50}\text{V}_{1.50}$ in NMPF.

2.5 Analysis with DFT Calculations

To understand how the discovered optimal element combinations work in NVMF, their electronic property is analyzed with DFT calculations. When we consider theoretical energy density of NMPF with 16 element combinations based on theoretical voltage profile, its cost effectiveness and toxicity, $\text{Mn}_{0.75}\text{V}_{1.25}$ and $\text{Co}_{0.50}\text{V}_{1.50}$ are suitable element combinations (Fig. 5a and Supplementary Fig. S5). To determine the degree of electron acceptance on the NMPF

according to the sodium concentration, Bader charge analysis[30], which can analyze the degree of the charge transfer, is performed for element combinations. Fig. 5b and Supplementary Fig. 8 show the total amount of charge transferred to the element combination for NMPF with 16 element combinations. In all cases, the total amount of charge transferred to the element combination in NMPF is higher than transferred charge of the NVPF ($V_{2.00}$). This implies that one of the conditions for working voltages to be within the voltage window is to accept more electrons than vanadium during sodiation as we mentioned before. Specifically, Fig. 5b and Supplementary Fig. 9 show atomic Bader charge analysis of the NMPF with element combinations containing vanadium ($Mn_{0.75}V_{1.25}$, $Co_{0.50}V_{1.50}$ and $Pd_{1.25}V_{0.75}$). The rhombus represents the charge transferred to each transition metal, and the black line is the average value of the transferred charge of V in NVPF ($V_{2.00}$). The amount of charge transferred to vanadium in the Na_1 , Na_2 , and Na_3 phases is similar to transferred charge of pure NVPF (V in $V_{2.00}$), but there is different in the Na_4 phase. This suggests that during the formation of the Na_4 (sodium excess phase) are unstable due to a lot of transferred charge to vanadium, but the NMPF with element combinations is energetically stable by transferring the charge to a substituted transition metal that can more readily accept the charge rather than vanadium.

3. Conclusions

In this study, we propose an algorithm to discover element combinations based on element mapping to address the limitation that the Gaussian process, which is a surrogate model for Bayesian optimization, can't take elements which are discontinuous as input. By assigning elements to continuous values through element mapping, it is possible to construct a chemical space for applying Bayesian optimization. Specifically, a unary score is presented that is highly correlated with a scoring function, which facilitates the formation of easily predictable (smooth) chemical space. It also revealed the importance of the correlation between scoring function and input by conducting element mapping through electronegativity and atomic number as well as unary score in terms of constructing the chemical space.

The main advantage of this proposed algorithm lies in its ability to efficiently explore low-dimensional chemical spaces with minimal observations. Unlike deep learning-based grid search methods that require extensive training data and computational resources for training, our approach does not require initial training data and resources for training. It is also flexible and scalable to a wide range of material systems by defining the scoring function and input appropriately.

Through this algorithm, we design a high-capacity cathode material of sodium ion batteries based on the NASICON structure based on element combinations ($\text{Mn}_{0.75}\text{V}_{1.25}$ and $\text{Co}_{0.50}\text{V}_{1.50}$) which can stabilize the sodium excess phase of NVPF. In conclusion, this work presents a robust, extensible and flexible framework for data-driven material design by combining Bayesian optimization and element mapping.

Computational details

Using the Vienna Ab initio Simulation Package (VASP)[31] with the projector-augmented wave (PAW) scheme and spin-polarization, calculations were conducted following the Perdew–Burke–Ernzerhof (PBE) formulation[32]. A plane-wave expansion of wave functions was set with a cutoff energy of 500 eV, and a Monkhorst–Pack method[33] employing a $1 \times 1 \times 1$ k-point grid was utilized. Convergence criteria for electronic and ionic steps in DFT calculations during observations in Bayesian optimization were 1.0×10^{-4} eV and 1.0×10^{-3} eV, respectively. For the validation of the NMPF with discovered element combinations, the convergence criteria were set at 1.0×10^{-6} eV and -0.02 eV/Å. Hubbard U terms[34] were applied to V, Cr, Mn, Fe, Co, Ni, Cu and Zn for 3.1, 3.5, 4.0, 4, 3.3, 6.4, 4.0 and 7.5, respectively[35]. The crystal structures were drawn with VESTA[36] software. In the Bayesian optimization algorithm, Gaussian process[13] which is a probabilistic machine learning model was used as the surrogate model with Matérn[12] kernel and an upper confidence bound (UCB) algorithm[37] is adopted for the acquisition function, which determines the maximum value of upper bound on uncertainty from Gaussian process regression.

Reference

1. Hwang, J.Y., S.T. Myung, and Y.K. Sun, *Sodium-ion batteries: present and future*. Chem Soc Rev, 2017. **46**(12): p. 3529-3614.
2. Zhao, L., et al., *Engineering of Sodium-Ion Batteries: Opportunities and Challenges*. Engineering, 2023. **24**: p. 172-183.
3. Xiang, X., K. Zhang, and J. Chen, *Recent Advances and Prospects of Cathode Materials for Sodium-Ion Batteries*. Adv Mater, 2015. **27**(36): p. 5343-64.
4. Xu, C., et al., *A Novel NASICON-Typed $\text{Na}_4\text{VMn}_0.5\text{Fe}_0.5(\text{PO}_4)_3$ Cathode for High-Performance Na-Ion Batteries*. Advanced Energy Materials, 2021. **11**(22).
5. Zhu, C., et al., *A High Power-High Energy $\text{Na}_3\text{V}_2(\text{PO}_4)_2\text{F}_3$ Sodium Cathode: Investigation of Transport Parameters, Rational Design and Realization*. Chemistry of Materials, 2017. **29**(12): p. 5207-5215.
6. Anantharamulu, N., et al., *A wide-ranging review on Nasicon type materials*. Journal of Materials Science, 2011. **46**(9): p. 2821-2837.
7. Wang, M., et al., *Synthesis and electrochemical performances of $\text{Na}_3\text{V}_2(\text{PO}_4)_2\text{F}_3/\text{C}$ composites as cathode materials for sodium ion batteries*. RSC Adv, 2019. **9**(53): p. 30628-30636.
8. Yan, G., et al., *Higher energy and safer sodium ion batteries via an electrochemically made disordered $\text{Na}_3\text{V}_2(\text{PO}_4)_2\text{F}_3$ material*. Nat Commun, 2019. **10**(1): p. 585.
9. Brochu, E., V.M. Cora, and N.d. Freitas, *A Tutorial on Bayesian Optimization of Expensive Cost Functions, with Application to Active User Modeling and Hierarchical Reinforcement Learning*. arXiv:1012.2599, 2010.
10. Frazier, P.I., *A Tutorial on Bayesian Optimization*. arXiv:1807.02811, 2018.
11. Snoek, J., H. Larochelle, and R.P. Adams, *PRACTICAL BAYESIAN OPTIMIZATION OF MACHINE LEARNING ALGORITHMS*. arXiv:1206.2944, 2012.
12. Rasmussen, C.E. and C. Williams, *Gaussian Processes for Machine Learning*. 2006: MIT Press.
13. Gramacy, R.B., *Surrogates-Gaussian Process Modeling, Design, and Optimization for the Applied Sciences*. 2020: CRC Press.
14. Kim, M., et al., *Searching for an Optimal Multi-Metallic Alloy Catalyst by Active Learning Combined with Experiments*. Adv Mater, 2022. **34**(19): p. e2108900.
15. Pedersen, J.K., et al., *Bayesian Optimization of High-Entropy Alloy Compositions for Electrocatalytic Oxygen Reduction**. Angew Chem Int Ed Engl, 2021. **60**(45): p. 24144-24152.
16. Khatamsaz, D., et al., *Bayesian optimization with active learning of design*

- constraints using an entropy-based approach.* npj Computational Materials, 2023. **9**(1).
17. Nugraha, A.S., et al., *Mesoporous trimetallic PtPdAu alloy films toward enhanced electrocatalytic activity in methanol oxidation: unexpected chemical compositions discovered by Bayesian optimization.* Journal of Materials Chemistry A, 2020. **8**(27): p. 13532-13540.
 18. Kusne, A.G., et al., *On-the-fly closed-loop materials discovery via Bayesian active learning.* Nat Commun, 2020. **11**(1): p. 5966.
 19. Shim, Y., et al., *Data-Driven Design of NASICON-Type Electrodes Using Graph-Based Neural Networks.* Batteries & Supercaps, 2024.
 20. Bai, Q., et al., *Computational Studies of Electrode Materials in Sodium-Ion Batteries.* Advanced Energy Materials, 2018. **8**(17).
 21. Zhao, D., et al., *Machine-learning-assisted modeling of alloy ordering phenomena at the electronic scale through electronegativity.* Applied Physics Letters, 2024. **124**(11).
 22. Li, Z., X. Ma, and H. Xin, *Feature engineering of machine-learning chemisorption models for catalyst design.* Catalysis Today, 2017. **280**: p. 232-238.
 23. Noh, J., et al., *Active learning with non-ab initio input features toward efficient CO(2) reduction catalysts.* Chem Sci, 2018. **9**(23): p. 5152-5159.
 24. Xie, T. and J.C. Grossman, *Crystal Graph Convolutional Neural Networks for an Accurate and Interpretable Prediction of Material Properties.* Phys Rev Lett, 2018. **120**(14): p. 145301.
 25. Cheng, G., X.G. Gong, and W.J. Yin, *Crystal structure prediction by combining graph network and optimization algorithm.* Nat Commun, 2022. **13**(1): p. 1492.
 26. Chen, C. and S.P. Ong, *A universal graph deep learning interatomic potential for the periodic table.* Nat Comput Sci, 2022. **2**(11): p. 718-728.
 27. Chen, C., et al., *Graph Networks as a Universal Machine Learning Framework for Molecules and Crystals.* Chemistry of Materials, 2019. **31**(9): p. 3564-3572.
 28. Gomez-Bombarelli, R., et al., *Automatic Chemical Design Using a Data-Driven Continuous Representation of Molecules.* ACS Cent Sci, 2018. **4**(2): p. 268-276.
 29. Iwasaki, Y., et al., *Efficient autonomous material search method combining ab initio calculations, autoencoder, and multi-objective Bayesian optimization.* Science and Technology of Advanced Materials: Methods, 2022. **2**(1): p. 365-371.
 30. Tang, W., E. Sanville, and G. Henkelman, *A grid-based Bader analysis algorithm without lattice bias.* J Phys Condens Matter, 2009. **21**(8): p. 084204.

31. Kresse, G. and J. Furthmüller, *Efficient iterative schemes for ab initio total-energy calculations using a plane-wave basis set*. Physical Review B, 1996. **54**: p. 169-186.
32. Perdew, J.P., K. Burke, and M. Ernzerhof, *Generalized Gradient Approximation Made Simple*. Physical Review Letters, 1996. **77**: p. 3865-3868.
33. Monkhorst, H.J. and J.D. Pack, *Special points for Brillouin-zone integrations*. Physical Review B, 1976. **13**(12): p. 5188-5192.
34. Dudarev, S.L., et al., *Electron-energy-loss spectra and the structural stability of nickel oxide: An LSDA+U study*. Physical Review B, 1998. **57**: p. 1505-1509.
35. Wang, L., T. Maxisch, and G. Ceder, *Oxidation energies of transition metal oxides within the GGA+U framework*. Physical Review B, 2006. **73**(19).
36. Momma, K. and F. Izumi, *VESTA: a three-dimensional visualization system for electronic and structural analysis*. Journal of Applied Crystallography, 2008. **41**(3): p. 653-658.
37. Agrawal, R., *Sample Mean Based Index Policies with $O(\log n)$ Regret for the Multi-Armed Bandit Problem*. Advances in Applied Probability, 1995. **27**: p. 1054-1078.